A&A 586, A115 (2016)
DOI: 10.1051/0004-6361/201527825

Astronomy & Astrophysics

Low-density laboratory spectra near the He II λ304 line⋆

Elmar Träbert[1,2], Peter Beiersdorfer[1], Nancy S. Brickhouse[3], and Leon Golub[3]

[1] Physics Division, Physical and Life Sciences, Lawrence Livermore National Laboratory, Livermore, CA 94550-9234, USA
e-mail: traebert@astro.rub.de; beiersdorfer1@llnl.gov
[2] Astronomisches Institut, Fakultät für Physik und Astronomie, Ruhr-Universität Bochum, 44780 Bochum, Germany
[3] Harvard-Smithsonian Center for Astrophysics, Cambridge, MA 02138, USA

Received 24 November 2015 / Accepted 31 December 2015

ABSTRACT

Aims. To interpret the EUV spectra of the solar corona, one hopes for laboratory data of specific chemical elements obtained under coronal conditions.
Methods. EUV spectra of He, C, N, O, F, Ne, S, Ar, Fe, and Ni in a 40 Å wide wavelength interval near λ304 were excited in an electron beam ion trap.
Results. We observe some two hundred lines about half of which are not yet identified and included in spectral models.
Conclusions. Our data provide a check on the atomic data bases underlying the spectral models that are used to interpret solar corona data. However, a multitude of mostly weak additional lines taken together represent a flux that is comparable to that of various primary lines.

Key words. Sun: corona – atomic data – methods: laboratory: atomic – techniques: spectroscopic – Sun: UV radiation

1. Introduction

The extreme ultraviolet (EUV) spectral range has been recognized as a wavelength range of utmost importance for solar coronal studies since sounding rockets and satellite missions have lifted spectrometers beyond the EUV-blocking Earth atmosphere. A classical example is the spectroheliograph aboard Skylab (for spectra, see Dere 1978), another one the Extreme Ultraviolet Imaging Telescope (EIT) aboard the SOHO spacecraft. One of the dominant spectral features in the middle of the EUV range is the 1s−2p resonance transition of He II. This line is bright, because He is highly abundant; its first ionization stage is easily produced, and the 2p resonance level is easily excited. For EUV spectroscopy of the corona this prominence is a boon and a bane: on one hand, the signal of this emission line is so bright that it outshines all other emission in the spectral neighborhood, on the other, it thus hides other lines. In fact, a spectrally poorly resolving instrument of moderate detection efficiency is enough to exploit this situation for monitoring the Sun's overall emission in the EUV and providing a reference signal. In this vein, one of seven EUV observation channels of the Solar Dynamics Observatory (SDO) Atmospheric Imaging Assembly (AIA) suite of instruments (see Pesnell et al. 2012 and subsequent articles for a comprehensive description of this spacecraft) is dedicated to this role of providing a reference for the observations in the six others (λ94, 131, 171, 193, 211, 335) that target specific lines of various ions of iron, so that in combination the signals can be exploited for determining the temperatures of coronal features in a range that spans several decades.

Another example for the ongoing interest in this wavelength band is NASA's Extreme Ultraviolet Normal Incidence Spectrograph (EUNIS; Thomas & Davila 2001) (a successor to the SERTS instrument) that is being flown on sounding rockets; for a number of measurement campaigns, one of the two channels has been covering the wavelength band 300−370 Å. This instrument operates at a spectral resolution close to ours (discussed below) which allows it to resolve lines close to the bright helium line He II λ304 (Brosius et al. 2008).

Any meaningful interpretation of the raw data garnered by SDO/AIA depends on extensive modeling (O'Dwyer et al. 2010; Parenti et al. 2012), guided, for example, by the CHIANTI database (Dere et al. 1997, 2009; Landi et al. 2012, 2013; Del Zanna et al. 2015). Parenti et al. (2012) demonstrate models that assign a larger role to contributions from lighter elements such as oxygen and neon than do the simulations by O'Dwyer et al. (2010). We have already presented detailed spectroscopic studies of the lines in the λ131, λ193, and λ211 SDO/AIA bands (Träbert et al. 2014a,b; Beiersdorfer et al. 2014b) in which we have checked on the wavelength literature data and have found many lines not yet in the literature.

Here we measure in the vicinity of the He II λ304 line. Even in well resolved spectra the foot of the outstandingly bright He II line is likely to mask the signal of other elements and ions in the spectral vicinity. However, it might well be interesting to see which spectral features are notably present "underneath" the He II λ304 line, which are revealed when the helium line is "switched off", as can be achieved in the laboratory. Moreover, the laboratory permits us to study the spectra of individual elements and have some control over their charge states, whereas observations of the solar corona face the dilemma of a distribution that comprises many elements. We have shown in the past (see, for example, Beiersdorfer et al. 1999a; Lepson et al. 2002) that laboratory measurements of spectra produced in an electron beam ion trap can be valuable in identifying features either missing from databases or not listed in their natural wavelength

⋆ Research supported by the Solar and Heliospherical Physics Program of the National Aeronautics and Space Administration under award NNH10AN31I.

positions. Thus our work should help to improve the databases and thus in turn also facilitate the interpretation of solar data.

The emission we have studied here is from the elements He, C, N, O, F, Ne, S, Ar, Fe, and Ni, most of which have a high solar abundance. Measurements of Mg and Si were intended as well, but had to be postponed because of technical problems.

2. Measurement

The measurements were performed at the Lawrence Livermore National Laboratory using the EBIT-I electron beam ion trap, a device that has been used for laboratory astrophysics measurements for over two decades (Beiersdorfer 2003). In this apparatus, a (quasi-) mono-energetic electron beam of adjustable energy serves to ionize and excite atoms under ultrahigh vacuum conditions. The residual gas pressure is lower than 10^{-11} mbar. Together with an electron density $n_e \leq 10^{12}$ cm^{-3} (Chen et al. 2004), the conditions approximate the dilute plasma conditions of the solar corona.

All the materials presently studied are introduced to the trap in gaseous form, some as atoms or simple molecules (CO_2, N_2, SF_6, Ne, Ar), others as a molecular vapor of a complex compound (iron as ironpentacarbonyl $Fe(CO)_5$, nickel as nickelocene $Ni(C_5H_5)_2$). The gas of interest is injected ballistically at reservoir pressures below 10^{-7} mbar into the ultrahigh vacuum of the EBIT vessel; the gas plume expands to a pressure well below 10^{-9} mbar where it traverses the actual trap volume and the electron beam (Träbert et al. 2000). Collisions with the electron beam disintegrate the molecules; any resulting positively charged particles are being trapped in the combination of electric and magnetic fields of a Penning trap plus the space charge effects caused by the electron beam. The trapped ions continue to be exposed to energetic electrons that collisionally excite and ionize the ions up to the limit imposed by the sequence of monotonically increasing ionization potentials. The electron beam energy therefore defines the maximum charge state that can be reached in the interplay of ionization and recombination, i. e., by electron capture or charge exchange (Beiersdorfer et al. 1990).

The gas flow is continuous, and low charge state ions are replenished all the time. Consequently there are contributions from low charge state ions in all spectra. In order to provide a rough discrimination of charge states, the present measurements were done at one to three electron beam energy settings (in the range 300 to 1000 eV) for most of the injected elements. However, the ionization potentials of most charge states of the light ions (CNOF) are so low that almost all can be highly ionized even at the lowest electron beam energies, which precludes any charge state discrimination of most of our unidentified lines of these species. On the other hand, the spectra of the few electron ions can be computed well; hence unidentified lines in these cases are likely to belong to ions with more than three electrons, which are less completely known. If one wanted to trace the actual production threshold in order to find out the ionization potential of the ion that produces a given spectral feature, one would have to increment the electron beam energy in much smaller steps than was done here (see Lepson et al. 2000, 2002, 2005).

For the present measurement, we used a medium-resolution flat-field grating spectrograph (FFS; Beiersdorfer et al. 1999b). The instrument was equipped with a 1200 ℓ/mm $R = 5$ m grating and operated at an angle of incidence of 87°. A cryogenically cooled CCD camera of 1340 × 1300 pixels of 20 μm × 20 μm each recorded the spectra. Similar instruments are currently functional at the NSTX, LTX, and Alcator tokamaks (Graf et al. 2008; Lepson et al. 2010, 2012, 2013).

Spectra were accumulated for 30 to 60 min each, filtered for cosmic ray events, and intercompared for irreproducible signal that might have passed the filtering process. The slightly quadratic calibration curve was adjusted by reference to known spectral lines mostly of light elements (He, N, O), as well as those of Fe (see Kelly 1987; Kramida et al. 2012).

Our spectrograph views the ion cloud in EBIT-I directly, and thus the spectral resolution is limited by instrumental parameters as well as the source size. The measured lines feature a width (FWHM) of about 300 mÅ which corresponds to a resolving power $R = \lambda/\Delta\lambda \approx 1100$ in first order of diffraction. This is a factor of three higher than what the MEGS-A grazing incidence grating spectrograph of the EVE experiment on board SDO achieves in this range (Woods et al. 2012) and a factor of 40 higher than the 12 Å FWHM band width covered by the λ304 channel of the AIA.

The line width of our grating spectrograph is almost independent of wavelength. Hence first and second diffraction order lines cannot be discriminated by line width. The strongest line at about half the wavelength of our present observations is the O VI line near λ150, and we see the second diffraction order image of this line near the position of the He II λ304 line. We therefore can estimate other candidates for second order line images in our present spectra based on their first-order strengths required to appear in higher orders of diffraction.

3. Data and analysis

The present measurements aim at a search for significant discrepancies between our observations and representative data bases used in well established solar spectrum modeling. As a basis for a comparison between our observations and the databases, we cite only wavelength data of lines listed in CHIANTI version 8 (the 2015 update from version 7.1 Dere et al. 1997; Landi et al. 2013; Del Zanna et al. 2015) or the NIST on-line database (Kramida et al. 2012) as "known" (though in many cases they differ significantly from each other). The NIST data tables have directly observed wavelengths as well as wavelengths deduced (via the Ritz principle) from energy levels (however determined), as well as results of computations. Unfortunately, neither set of measured, inferred, or computed wavelength data is complete, nor are the wavelengths and energy levels in the NIST data base necessarily consistent. We quote the individual NIST table wavelengths, whether directly measured or derived, by subjective choice. This ambiguity of wavelength data offered by the data base is smaller than our measurement uncertainty in the present study, but it underlines the need for continued spectroscopic investigation. CHIANTI is the prime reference for the spectrum simulations performed by O'Dwyer et al. (2010), and in a recent evaluation of iron lines (Beiersdorfer & Lepson 2012) it was found to be more reliable than the NIST database. Many lines we observe remain unidentified for now (except for the element). However, the wavelength accuracy of our measurements is sufficient to identify the known lines without problems; we thus assume that it is equally sufficient to provide guidance for the eventual identification of the unknown lines. Certainly, our measured wavelengths are more accurate than most calculations.

Relative line intensities are important for line identification purposes, and we list these for our measurements. However, the production of a given charge state depends on the electron beam energy and thus may differ drastically from one spectrum to the other, if an ionization threshold is being crossed within a series

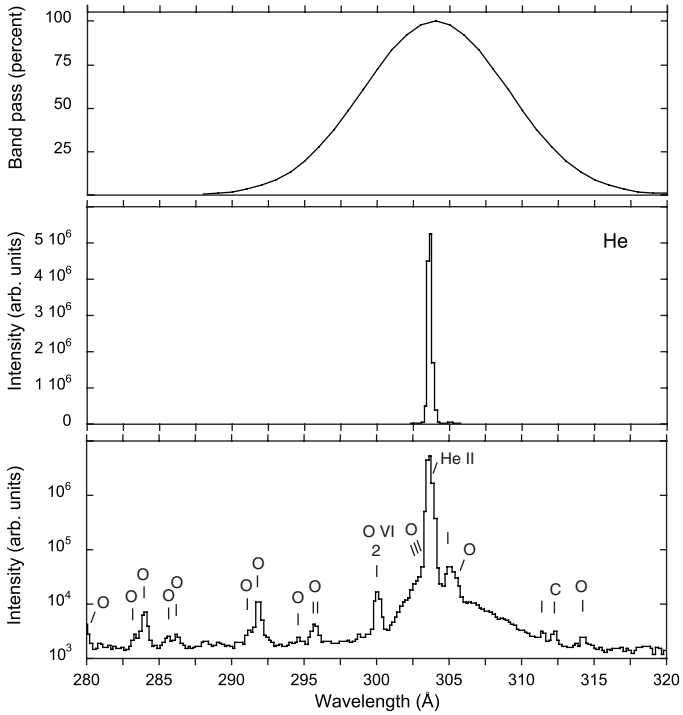

Fig. 1. Spectrum of helium in the range λ280–λ320 recorded at the EBIT-I electron beam ion trap at an electron beam energy of 1000 eV. The only line that is recognizable at this scale is the He II line at 303.78 Å. The band pass function of the SDO/AIA λ304 channel is indicated on *top*. The *bottom of the figure* shows the same spectrum on a logarithmic scale; at a level of more than three orders of magnitude weaker than the dominant helium line there are various oxygen lines in first and second diffraction order (marked by "2").

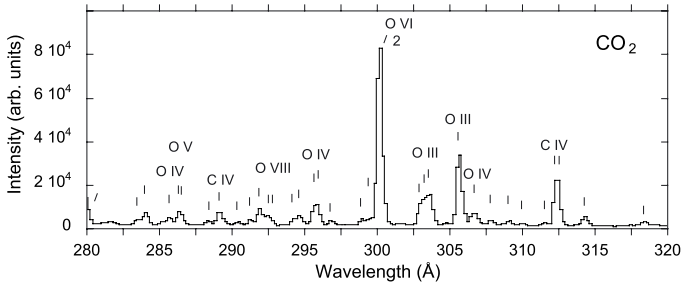

Fig. 2. Spectrum of carbon and oxygen in the range λ280–λ320: the spectrum was recorded at the EBIT-I electron beam ion trap at an electron beam energy of 700 eV. Identified spectral features are labeled by the corresponding spectrum. The oxygen line near 300 Å appears in second diffraction order (marked "2") .

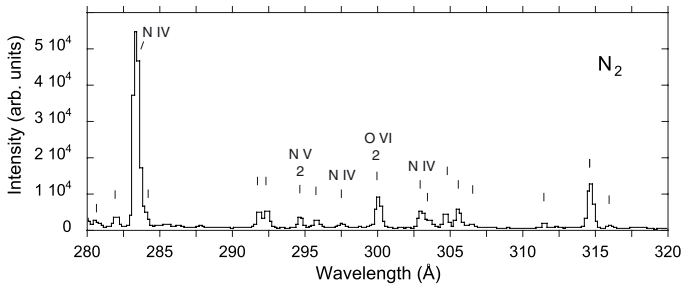

Fig. 3. Spectrum of nitrogen in the range λ280–λ320: the spectrum was recorded at the EBIT-I electron beam ion trap at an electron beam energy of 1000 eV. The line markers are visual aids only, because the actual number of line components that can be discerned in spectral line fits of blends may depend on the available spectral resolution. Identified spectral features are labeled by the corresponding spectrum. Lines that are recognized as second diffraction order images are marked "2".

of spectral recordings, or very little, if the beam energy exceeds the threshold to begin with. Hence meaningful relative line intensities can be derived from our spectra only for lines that are known to belong to the same ion species. Even at a resolving power of 1100, not all lines are resolved. A large number of insufficiently resolved weak lines may appear as a continuum underlying the spectrum, which may not be distinguishable from the free-bound or bremsstrahlung continuum. The problem of true and pseudo continua is compounded by the fact that the read-out noise of a CCD detector shows statistical fluctuations. Hence the relative intensities of weak lines are more uncertain than the straightforward statistical uncertainty of a fit result may suggest. We indicate gross relative line intensities, assigning a value of ten to the strongest line within the displayed spectrum. Such a relative intensity information within a given charge state from our measurements is sufficient to match the accuracy of theoretical modeling data and thus to help line identification, even if the theoretical data are shifted in wavelength.

Helium. The He II 1s-np resonance line series is helpful for wavelength calibrations $\lambda \leq 304$ Å. The 1s−2p λ303.78 line is so strong that in our spectra (Fig. 1) the spectral lines from indigenous ion species in the trap are not noticeable on a linear scale. The situation is very similar to that of the solar observations by the EUNIS instrument (Brosius et al. 2008). In the coronal spectra observed with EUNIS, strong lines of other elements have been measured within less than 1 Å from the He II line. Weaker lines show above the wide foot of the He II line only when several Ångströms away. A number of oxygen lines from the residual gas in EBIT have been seen in our spectra, which we discuss below, but these lines are several orders of magnitude weaker than the He II line in our device, and are noticeable only when the measured spectrum is displayed on a logarithmic scale (see Fig. 1). In Fig. 1 we also show the response of the 304 Å channel of the AIA on SDO, since this is one of the seven wavelength regions of interest of that instrument.

Carbon and *oxygen*. The spectral lists of NIST and CHIANTI have very few carbon lines that are expected to show up in our spectra; the brightest of these is the C IV 2s−3p transition multiplet at λ312.4, as seen in Fig. 2. By contrast, the lists have many more lines of oxygen, most of which we identify in our spectra (see Table A.1). Three $n = 3-4$ transitions lines of O VIII listed in CHIANTI v. 7.1 are no longer listed in version 8. Eighteen features in our spectra remain unidentified. We believe that these are from oxygen. It is, of course, possible that among the unidentified lines that we observe when injecting CO_2 there are lines that actually belong to carbon ions. The strongest line observed in the spectra is from the O VI line at λ150, which we observed in second order of diffraction.

Nitrogen. Spectra of nitrogen were obtained at an electron beam energy of 1000 eV (Fig. 3). The strongest nitrogen line in our spectral band is the N V 2p−3d triplet transition multiplet near λ283. In addition, we identify three other features and find 14 lines that remain unassigned. Known nitrogen lines and unidentified lines are given in Table A.2.

Fluorine and *sulfur*. Fluorine and sulfur were introduced into EBIT as the molecular gas SF_6. This implies that one does not immediately know whether an observed spectral line belongs to F or S. Fluorine is not very abundant in the sun, and no fluorine

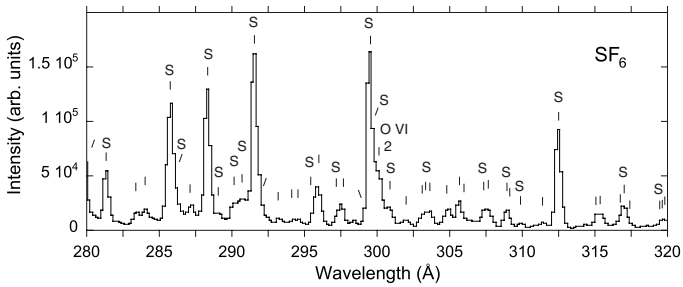

Fig. 4. Spectrum of fluorine and sulfur in the wavelength range λ280–λ320: the spectrum was recorded at the EBIT-I electron beam ion trap at an electron beam energy of 1000 eV. Visually recognized line positions are marked. The second diffraction order of a O VI line and the many known first-order sulfur lines are marked by their element symbol.

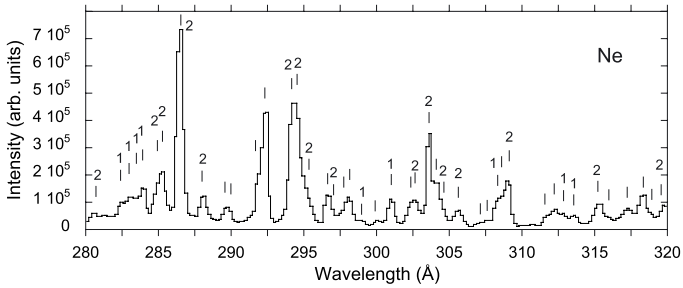

Fig. 5. Spectrum of neon in the range λ280–λ320: the spectrum was recorded at the EBIT-I electron beam ion trap at an electron beam energy of 1000 eV. Of the about 45 lines seen in this spectrum (with eye-guiding markers), known identifications are marked "1" and "2" for first and second diffraction order images.

lines are listed by CHIANTI. There are several significant wavelength changes from CHIANTI v. 7.1 to version 8 (for example for S XII, moving a number of wavelength values that previously differed from the NIST data close to the latter). These changes are much larger than the seeming reliability of the CHIANTI wavelength values which are listed with a last digit corresponding to ±0.1 mÅ.

Several known strong sulfur lines (near λ286, 288, 291, 299, 312) are known to fall into our wavelength band and we identify them readily (see Table A.3). Moreover, our spectra, recorded at electron beam energies of 300, 600, and 1000 eV, show quite a number of additional unidentified lines that we assume to also belong to sulfur (Fig. 4). A S XII line is known at λ297.4; our spectra, however, show a line width that is better explained by two lines of similar intensity. The second line, at λ297.6, presently remains unidentified. Similarly the known S XIII line at λ307.4 is accompanied by a second, presently unidentified, line within the common wider line profile, as is the S XIII line at λ316.8.

Neon. Neon spectra were recorded at electron beam energies of 300, 600, and 1000 eV. A sample spectrum is shown in Fig. 5. Known and observed lines are given in Table A.4. Quite a number of lines are seen in our spectra. Only about a dozen of the weaker lines are listed in the NIST and CHIANTI tables as belonging to Ne III in first diffraction order. However, many other lines coincide with the second diffraction order positions of known Ne II through Ne V lines.

Argon. Neither the NIST database nor CHIANTI has prominent Ar lines in the λ280–320 wavelength band. Actually, among the two databases, just two Ar VI lines are known in

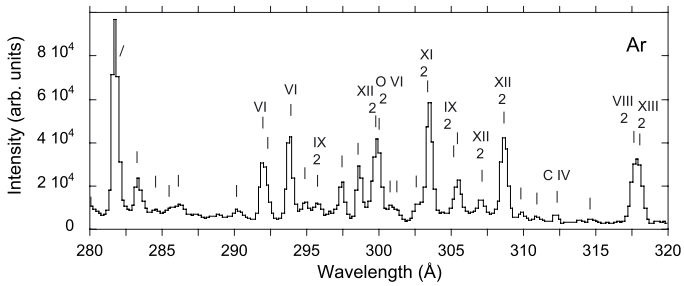

Fig. 6. Spectrum of argon in the range λ280–λ320: the spectrum was recorded at the EBIT-I electron beam ion trap at an electron beam energy of 1000 eV. Eye-guiding markers indicate visual line positions. Known Ar lines are labeled by the spectrum number, while contamination lines from carbon and oxygen are labeled by the element. Lines that appear in second order of diffraction are marked by "2".

this wavelength interval and listed in the NIST tables, whereas CHIANTI does not provide any data on Ar VI at all. Owing to our use of a grating spectrograph, we also expect second diffraction order images of various Ar VIII to Ar XIII lines. Between CHIANTI versions 7.1 and 8, several wavelength entries have changed by some 20 mÅ, which may be considered a realistic uncertainty estimate, even as the CHIANTI tables list a last digit that corresponds to 0.1 mÅ. Our argon spectra were recorded at electron beam energies of 300, 600, and 1000 eV; for an example see Fig. 6. The spectra show about 50 lines that clearly vary with the electron beam energy. Many of these lines, however, appear in second diffraction order. Among these are lines of O V and O VI, as well as a first diffraction order line of C IV. One of the two strongest lines we see (near 281.9 Å) is not known from the literature. The NIST tables name Ar VI and Ar VII lines near this position, but those lines do not connect to the ground configuration and thus are unlikely candidates for strong lines in low-density environments. The Ar lines we observe are given in Table A.5.

Iron. Iron was studied at six electron beam energies from 300 to 2600 eV. In our λ280−320 spectra (see sample spectrum in Fig. 7), the brightest line by far is the Fe XV line at 284 Å. A multitude of much weaker lines (see the lower part of Fig. 7, in which the spectrum is displayed on a logarithmic scale) cluster near λ304, where in the solar corona those lines would be dwarfed by the He II λ304 line. Our sample spectrum contains about 45 lines in an interval merely 40 Å wide. It is no surprise then that many of these lines are blended with others.

We note that in our spectra (with continuous gas injection) there are many unidentified weak lines. However, since the iron-carrying molecule that we use for injecting Fe into the trap, iron-pentacarbonyl, is also containing oxygen, one has to be aware of blending with lines from oxygen. Indeed, many of the weak structures seen in our Fe spectra coincide with oxygen lines (see Fig. 2). On the other hand the overall spectral shape is not the same as that produced by CO_2 injection. The NIST and CHIANTI reference tables together list about 90 Fe lines in this wavelength interval, however, most lines in this range appear in only one of the tables and not the other. In cases where both tables have entries, the entries agree in some cases, but differ by up to 80 mÅ in other cases. With our present instrument we cannot resolve the wavelength discrepancies between the two databases. Therefore, we refrain from showing and discussing the literature data for Fe beyond the two examples in Table A.6. This spectral region will need to be investigated with very high resolution

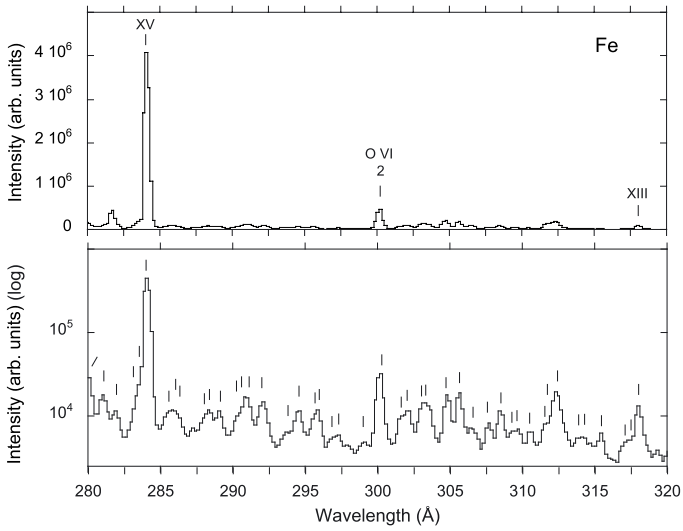

Fig. 7. Spectrum of iron in the range λ280–λ320: the spectrum was recorded at the EBIT-I electron beam ion trap at an electron beam energy of 1000 eV. The *lower part* of the figure shows the spectrum in a logarithmic display. Fiducial markers indicate 45 line positions as judged visually at this spectral resolution. Only two of the many iron lines known in this wavelength range can be unambiguously assigned in this spectrum and are labeled by the spectrum number.

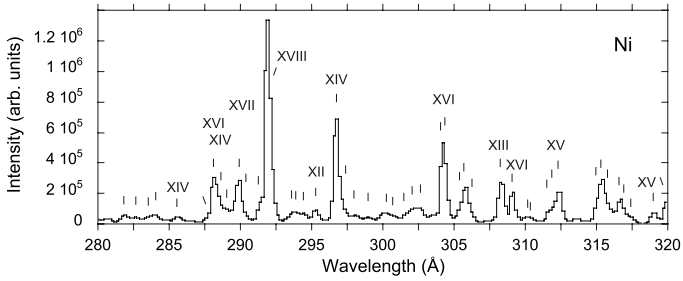

Fig. 8. Spectrum of nickel in the range λ280–λ320: the spectrum was recorded at the EBIT-I electron beam ion trap at an electron beam energy of 1000 eV. Fiducial markers indicate the rich structure of the spectrum, without being complete. Only the strongest of the known lines are identified by the spectrum number.

and small steps in the electron beam energy in the future, especially as new instrumentation becomes available to investigate this spectral region with very high resolution (Beiersdorfer et al. 2014a).

Nickel. Nickel spectra have been observed at electron beam energies of 300, 600, 1000, and 1600 eV. Similar to the case of Fe, we see little of the known low or very high charge state lines. For example, for Ni XIX CHIANTI tables list practically only lines predicted from theoretical energy levels (and thus with some wavelength uncertainty) in a wide range of the EUV spectral band. Five of these Ni XIX lines in CHIANTI fall into our present wavelength band, but we do not recognize any of them in our spectra even at a beam energy of 1600 eV, at which the Ni^{18+} ion abundance is optimized. This is most likely the result of the fact that 3−3 lines from such high ionization states are very weak (the comparable lines in Fe XVII are essentially invisible; the 3s−3p transition in Fe XVII, for example, was discussed only in very high-resolution measurements on EBIT-I Beiersdorfer et al. 2014b).

A sample spectrum of nickel with many bright features is shown in Fig. 8. The present wavelength band evidently comprises a sizable number of prominent Ni lines, which are known and appear as first diffraction order images in our spectra. In addition, our spectra comprise many unidentified lines. Not all of these are weak, but some have intensities that are comparable to known lines. The wavelengths of our observed lines are given in Table A.7. This table also lists wavelengths from the NIST and CHIANTI databases, and the situation is similar to the one discussed above for iron: while there is agreement among the two databases in some cases, there is disagreement on the order of 100 mÅ in others. In addition, there are many cases in which only one or the other database has entries. Between CHIANTI versions 7.1 and 8, some wavelength entries for highly charged Ni ions change by 70 mÅ, generally closer to the NIST data entries. The latter are given with fewer decimals, but apparently more realistically. Evidently, knowledge of the highly charged ion spectra of nickel is far from complete.

4. Discussion

The present measurements at an electron beam ion trap demonstrate how many unidentified lines of a few given elements appear in survey spectra recorded under conditions that resemble many astrophysical plasmas. The present spectra illustrate the need for additional work, especially for iron and nickel. Ideally, such work should be carried out with higher spectral resolution and finer electron beam energy steps, in order to provide additional information to aid possible identification of the many unknown new features we have listed in our tables.

Overall, we observe more than 200 spectral lines in the wavelength band of present interest. About half of the lines cannot be identified from the NIST and CHIANTI databases, the latter of which is a primary resource for the interpretation of solar data. While most of the new lines are individually weak, when taken together they represent a flux that resembles the flux of various stronger lines that are used in spectral models. Thus the solar data interpretation might benefit from an at least approximate inclusion of the many new lines.

Acknowledgements. This work was performed under the auspices of the US Department of Energy by Lawrence Livermore National Laboratory under Contract DE-AC52-07NA27344. E.T. acknowledges support from the German Research Association (DFG) (grants Tr171/18 and Tr171/19).

References

Beiersdorfer, P. 2003, ARA&A, 41, 343
Beiersdorfer, P., & Lepson, J. K. 2012, ApJS, 201, 28
Beiersdorfer, P., Osterheld, A. L., Chen, M. H., et al. 1990, Phys. Rev. Lett., 65, 1995
Beiersdorfer, P., Lepson, J. K., Brown, G. V., et al. 1999a, ApJ, 519, L185
Beiersdorfer, P., Crespo López-Urrutia, J. R., Springer, P., Utter, S. B., & Wong, K. L. 1999b, Rev. Sci. Instr., 70, 276
Beiersdorfer, P., Magee, E. W., Brown, G. V., et al. 2014a, Rev. Scient. Instr., 85, 11E422
Beiersdorfer, P., Träbert, E., Lepson, J. K., Brickhouse, N. S., & Golub, L. 2014b, ApJ, 788, 25
Brosius, J. W., Rabin, D. M., Thomas, R. J., & Landi, E. 2008, ApJ, 677, 781
Chen, H., Beiersdorfer, P., Heeter, L. A., et al. 2004, ApJ, 611, 598
Del Zanna, G., Dere, K. P., Young, P. R., Landi, E., & Mason, H. E. 2015, A&A, 582, A56
Dere, K. P. 1978, ApJ, 221, 1062
Dere, K. P., Landi, E., Mason, H. E., Monsignori Fossi, B. C., & Young, P. R. 1997, A&AS, 125, 149

Dere, K. P., Landi, E., & Young, P. R. 2009, A&A, 498, 915
Graf, A. T., Brockington, S., Horton, R., et al. 2008, Canad. J. Phys., 86, 307
Kelly, R. L. 1987, J. Phys. Chem. Ref. Data, 16, 1
Kramida, A., Ralchenko, Yu., Reader, J., & NIST ASD team 2012, NIST Atomic Spectra Database, ver. 5.0, Online, Available: http://physics.nist.gov/asd [2012, October 3]. National Institute of Standards and Technology, Gaithersburg, MD, USA
Landi, E., Del Zanna, G., Young, P. R., Dere, K. P., & Mason, H. E. 2012, ApJS, 744, 99
Landi, E., Young, P. R., Dere, K. P., Del Zanna, G., & Mason, H. E. 2013, ApJS, 763, 86
Lepson, J. K., Beiersdorfer, P., Brown, et al. 2000, Rev. Mex. Astron. Astrophys., 9, 137
Lepson, J. K., Beiersdorfer, P., Brown, G. V., et al. 2002, ApJ, 578, 648
Lepson, J. K., Beiersdorfer, P., Behar, E., & Kahn, S. M. 2005, Nucl. Instr. Meth. B, 235, 131
Lepson, J. K., Beiersdorfer, P., Clementson, J., et al. 2010, J. Phys. B, 43, 144018
Lepson, J. K., Beiersdorfer, P., Clementson, J., et al. 2012, Rev. Scient. Instr., 83, 10D520
Lepson, J. K., Beiersdorfer, P., Bitter, M., Roquemore, A. L., & Kaita, R. 2013, Phys. Scr., T156, 014075
O'Dwyer, B., Del Zanna, G., Mason, H. E., Weber, M. A., & Tripathi, D. 2010, A&A, 521, A21
Parenti, S., Schmieder, B., Heinzel, P., & Golub, L. 2012, ApJ, 754, 66
Pesnell, W. D., Chamberlin, P. C., & Thompson, B. J. 2012, Sol. Phys., 275, 3
Thomas, R. J., & Davila, J. M. 2001, Proc. SPIE, 4498, 161
Träbert, E., Beiersdorfer, P., Utter, S. B., et al. 2000, ApJ, 541, 506
Träbert, E., Beiersdorfer, P., Brickhouse, N. S., & Golub, L. 2014a, ApJS, 211, 14
Träbert, E., Beiersdorfer, P., Brickhouse, N. S., & Golub, L. 2014b, ApJS, 215, 6
Woods, T. N., Eparvier, F. G., Hock, R., et al. 2012, Sol. Phys., 275, 115

Appendix A: Tables

Table A.1. Lines observed in EBIT within the wavelength band λ280 to λ320 when injecting CO_2.

Spectrum	Transition type	Line intensity	λ (Å) This work	Unc. (mÅ)	λ (Å) CHIANTI[a]	λ (Å) NIST[b]
Known carbon lines						
C IV	2p−4d	blended	…	…	289.1409	289.141
C IV	2p−4d	0.7	289.21	100	289.2277	289.228
C IV	2p−4d	blended	…	…	289.2310	289.231
C IV	2p−4s	blended	…	…	296.8556	296.856
C IV	2p−4s	0.15	296.9	150	296.9506	296.951
C IV	2s−3p	3	312.4	100	312.4202	312.420
C IV	2s−3p	blended	…	…	312.4511	312.451
Known oxygen lines						
O IV	2p−3d	0.4	285.7	150	285.7100	285.71
O IV	2p−3d	blended	…	…	285.8340	285.84
O V	$2p^2$−2s3p	0.7	286.47	100	286.4485	286.448
O VIII	3s−4p	blended	…	…	292.4658	…
O VIII	3p−4s	0.45	292.6	100	292.5997	…
O VIII	3p−4s	…	…	…	292.9814	…
O IV	2p−3s	…	…	…	295.6580	295.658
O IV	2p−3s	blended	…	…	295.6670	295.667
O IV	2p−3s	1.25	295.82	100	295.8710	295.871
O IV	2p−3s	blended	…	…	295.8800	295.880
O III	2p−3s	…	…	…	…	295.942
O VI	2p−3s	10	300.2	100	150.0893 (II)	150.089 (II)
O VI	2p−3s	blended	…	…	150.1250 (II)	150.125 (II)
O III	2p−3d	1.9	303.6	100	303.4130−303.8000	303.41−303.80
O III	2p−3d	4	305.7	100	305.5960−305.8360	305.596−305.882
O IV	3p−3s	0.7	306.7	100	306.6210−306.8840	306.621−306.884
O III	2p−3d	…	…	…	308.3050	…
O IV	2p−3s	blended	…	…	311.4990	311.499
O IV	2p−3s	0.1	311.6	150	…	311.682
O IV	2p−3s	blended	…	…	311.7350	311.735
Unidentified lines						
…	…	1.5	280.0	150	…	…
…	…	0.2	283.6	150	…	…
…	…	0.6	284.1	150	…	…
…	…	0.15	288.4	150	…	…
…	…	0.06	290.5	200	…	…
…	…	0.2	291.3	150	…	…
…	…	0.8	291.9	150	…	…
…	…	0.2	294.3	150	…	…
…	…	0.4	294.7	150	…	…
…	…	0.2	296.9	150	…	…
…	…	0.2	298.8	150	…	…
…	…	0.3	299.2	150	…	…
…	…	2.0	303.1	100	…	…
…	…	0.22	307.8	150	…	…
…	…	0.2	309.1	150	…	…
…	…	0.04	310.1	200	…	…
…	…	0.45	314.3	150	…	…
…	…	0.2	318.4	150	…	…

Notes. The unknown lines may technically originate in spectra up to C VI or O VII.

References. [(a)] From the CHIANTI database v. 7.1 and v.8 (Del Zanna et al. 2015); [(b)] from the on-line database at NIST (Kramida et al. 2012) .

Table A.2. Nitrogen lines observed in EBIT within the wavelength band λ280 to λ320.

Spectrum	Transition type	Line intensity	λ (Å) This work	Unc. (mÅ)	λ (Å) CHIANTI[a]	λ (Å) NIST[b]
Known nitrogen lines						
IV	2p−3d	10	283.4	100	283.4170−283.5840	283.42−283.58
IV	2p−4s	…	…	…	…	289.479
V	2s−5p	0.5	294.7	150	147.4240−147.4273	147.424−147.427 (II)
IV	2p−3d	0.2	297.5	200	…	297.597−297.817
IV	2p−3d	0.7	303.0	150	…	303.013−303.280
Unidentified lines						
…	…	0.2	280.8	200	…	…
…	…	0.4	282.1	200	…	…
…	…	0.6	284.1	100	…	…
…	…	0.1	285.6	150	…	…
…	…	0.1	287.7	150	…	…
…	…	0.6	291.9	150	…	…
…	…	0.7	292.4	150	…	…
…	…	0.3	295.8	150	…	…
…	…	0.3	303.6	150	…	…
…	…	0.6	304.7	150	…	…
…	…	0.9	305.6	100	…	…
…	…	0.2	306.8	150	…	…
…	…	0.2	311.5	150	…	…
…	…	2.2	314.7	100	…	…

Notes. The unknown nitrogen lines may technically originate in spectra up to N VII.

References. [(a)] From the CHIANTI database v.8 (Del Zanna et al. 2015); [(b)] from the on-line database at NIST (Kramida et al. 2012).

Table A.3. Fluorine or sulfur lines observed in EBIT within the wavelength band λ280 to λ320.

Spectrum	Transition type	Line intensity	λ (Å) This work	Unc. (mÅ)	λ (Å) CHIANTI[a]	λ (Å) NIST[b]
Known sulfur lines						
S X	2s−2p	0.8	280.3	100	280.3576	280.34
S XI	2s−2p	2.6	281.4	100	281.4021	281.40
S XI	2s−2p	…	…	…	…	281.63
S X	2s−2p	…	…	…	282.2066	282.206
S XI	2s−2p	…	…	…	…	285.49
S XI	2s−2p	…	…	…	285.5875	285.58
S XI	2s−2p	7	285.8	100	285.8226	285.82
S XI	2s−2p	blended	…	…	285.8463	285.85
S XI	2s−2p	blended	…	…	…	285.88
S V	3s−4p	blended	…	…	…	286.095
S V	3s−4p	0.8	286.4	150	…	286.401
S XII	2s−2p	8	288.3	100	288.4340	288.416
S VI	3p−4d	blended	…	…	…	289.067
S VI	3p−4d	0.6	289.1	150	289.0810	289.082
S X	2s−2p	blended	…	…	289.3817	289.4
S VI	3p−4d	2	290.2	100	290.1270	290.127
S VI	3p−4d	blended	…	…	290.1420	290.142
S XII	2s−2p	2.4	290.8	100	290.8840	290.88
S XII	2s−2p	blended	…	…	291.1420	291.142
S XII	2s−2p	blended	…	…	291.3670	291.367
S XI	2s−2p	10	291.6	100	291.5661	291.57
S XI	2s−2p	blended	…	…	291.5780	291.58
S XII	2s−2p	blended	…	…	291.6260	291.63
S XI	2s−2p	blended	…	…	291.8112	291.81
S XI	2s−2p	0.25	295.6	200	295.6093	295.61
S XII	2s−2p	0.8	297.4	150	297.4200	297.396
S XII	2s−2p	9.5	299.5	100	299.5180	299.518

Notes. There are no known fluorine lines in this interval. Known sulfur lines are marked by the elemental symbol. The unknown lines may technically originate in spectra up to F VII or S XII.

References. [(a)] From the CHIANTI database v.8 (Del Zanna et al. 2015); [(b)] from the on-line database at NIST (Kramida et al. 2012).

Table A.3. continued.

Spectrum	Transition type	Line intensity	λ (Å) This work	Unc. (mÅ)	λ (Å) CHIANTI[a]	λ (Å) NIST[b]
S XII	2s−2p	blended	...	...	299.7920	299.79
S XIII	2s−2p	1.7	300.1	100	299.9568	299.956
S XIII	2s−2p	1.5	300.8	150	300.9860	300.99
S XIII	2s−2p	blended	...	...	303.3848	303.384
S IX	2s−2p	1.4	303.7	100	...	303.7
S XIII	2s−2p	0.9	307.4	100	307.3883	307.388
S XIII	2s−2p	0.7	308.9	150	308.9534	308.953
S X	2s−2p	0.25	309.9	200	...	154.880 (II)
S XIII	2s−2p	7.4	312.5	100	312.7322	312.732
S XIII	2s−2p	0.95	316.7	150	316.8433	316.843
S V	3p−4d	0.8	319.6	150	...	319.487
S V	3p−4d	0.6	319.9	150	...	319.851
S V	3p−4d	blended	...	...	...	319.865
Unidentified lines						
...	...	4	279.9	100	...	...
...	...	0.2	283.4	200	...	...
...	...	0.6	284.6	150	...	...
...	...	1	287.2	100	...	...
...	...	0.55	292.1	150	...	...
...	...	0.23	293.3	200	...	...
...	...	0.33	294.4	200	...	...
...	...	0.33	294.7	200	...	...
...	...	3.3	295.9	100	...	...
...	...	0.95	297.6	100	...	...
...	...	0.24	298.4	200	...	...
...	...	0.4	302.0	150	...	...
...	...	1.8	304.9	100	...	...
...	...	0.9	305.6	100	...	...
...	...	0.5	306.2	150	...	...
...	...	0.95	307.7	100	...	...
...	...	0.7	308.9	150	...	...
...	...	0.35	311.4	200	...	...
...	...	1.5	315.1	100	...	...
...	...	1.1	315.5	100	...	...
...	...	0.2	316.3	200	...	...
...	...	1.7	317.4	100	...	...

Table A.4. Neon lines observed in EBIT within the wavelength band λ280 to λ320.

Spectrum	Transition type	Line intensity	λ (Å) This work	Unc. (mÅ)	λ (Å) CHIANTI[a]	λ (Å) NIST[b]
Known Ne lines						
IV	2p−5d	0.65	280.8	100	…	140.329−140.369 (II)
III	2p−3s	0.8	282.5	100	282.4910	282.495
III	2p−3s	0.8	283.0	100	283.1440	283.1392
III	2p−3s	blended	…	…	283.1670	283.1745
III	2p−3s	blended	…	…	283.6440	…
III	2p−3s	blended	…	…	283.6600	283.6651
III	2p−3s	1.2	284.0	100	283.8680	…
V	2p−3d	1.0	285.0	100	142.4350−142.6610 (II)	142.441−142.661 (II)
V	2p−3d	1.0	285.6	100	142.7240 (II)	142.724 (II)
V	2p−3d	10	286.6	100	143.2190−143.4480 (II)	143.219−143.408 (II)
IV	2p−5s	0.85	288.1	100	…	144.024−144.278 (II)
VIII	3d−4f	3.0	292.6	100	…	292.38−292.47
V	2p−3d	2.8	294.0	100	…	146.888 (II)
V	2p−3d	6.5	294.5	100	147.1320 (II)	147.138 (II)
VI	…	1.6	295.2	100	147.3320−147.5120 (II)	147.33−147.51 (II)
V	2p−3d	blended	…	…	148.7830 (II)	148.84 (II)
IV	2p−4d	0.62	297.4	150	…	148.9404 (II)
VIII	3p−4s	0.54	299.1	100	…	298.7; 299.1
III	2p−3s	1.0	301.2	100	301.1240	…
V	2p−3d	1.3	302.8	100	151.3760,151.4240 (II)	151.237, 151.424 (II)
V	2p−3d	blended	…	…	151.5820 (II)	…
IV	2p−4d	4.0	303.7	100	…	151.4946−151.8343 (II)
IV	2p−4d	0.57	304.6	150	…	152.2385, 152.2391 (II)
IV	3p−5s	0.8	305.6	100	…	152.663 (II)
III	2p−3s	1.3	308.5	100	308.5630	308.5720
V	2p−3d	2.5	309.0	100	…	154.520 (II)
V	2p−3d	…	…	…	156.618 (II)	…
III	2p−3s	0.56	312.9	100	313.0430	313.0574
III	2p−3s	0.55	313.6	100	313.6740	313.692
III	2p−3s	…	…	…	313.9480	313.964
IV	2p−4s	0.85	315.3	100	…	157.6386−157.8713 (II)
IV	2s−3p	1.1	319.7	100	…	159.8676−159.8729 (II)
Unidentified lines						
…	…	0.35	281.2	100	…	…
…	…	0.9	289.6	100	…	…
…	…	0.9	289.8	100	…	…
…	…	3.0	291.8	100	…	…
…	…	5.0	292.3	100	…	…
…	…	1.5	296.8	100	…	…
…	…	0.8	297.8	100	…	…
…	…	0.97	298.1	100	…	…
…	…	0.55	300.1	150	…	…
…	…	1.1	300.9	100	…	…
…	…	0.85	302.3	100	…	…
…	…	1.8	304.1	100	…	…
…	…	0.27	307.1	150	…	…
…	…	0.3	307.8	150	…	…
…	…	0.55	311.7	150	…	…
…	…	0.65	312.3	100	…	…
…	…	0.55	315.8	150	…	…
…	…	0.76	316.7	100	…	…
…	…	0.5	317.4	150	…	…
…	…	0.68	318.1	100	…	…
…	…	0.58	318.8	150	…	…

Notes. The unknown Ne lines may technically originate in spectra up to Ne IX.

References. [(a)] From the CHIANTI database v.8 (Del Zanna et al. 2015); [(b)] from the on-line database at NIST (Kramida et al. 2012).

Table A.5. Argon lines observed in EBIT within the wavelength band λ280 to λ320.

Spectrum	Transition type	Line intensity	λ (Å) This work	Unc. (mÅ)	λ (Å) CHIANTI[a]	λ (Å) NIST[b]
Known lines						
VI	3p−4s	2.7	292.1	100	...	292.134
VI	3p−4s	4.1	294.0	100	...	294.03
IX	3p−4d	0.72	295.9	150	147.9590 (II)	147.952 (II)
IX	3p−4d	...	...	...	148.4120 (II)	148.402 (II)
XII	2s−2p	1.35	299.7	150	149.9290 (II)	149.922 (II)
XI	2s−2p	4.7	303.6	100	151.8540 (II)	151.845 (II)
IX	3p−4d	1.5	...	...	152.5730 (II)	152.576 (II)
IX	3p−4d	blended	...	...	152.6320 (II)	...
IX	3p−4d	blended	...	...	152.6820 (II)	...
IX	3p−4d	1.85	305.6	100	152.6970 (II)	152.690 (II)
XII	2s−2p	1.1	307.2	150	153.6280 (II)	153.624 (II)
IX	3p−4d	...	...	...	153.7060 (II)	153.727 (II)
IX	3p−4d	...	...	...	154.0580 (II)	154.106 (II)
XII	2s−2p	4.2	308.8	100	154.4220 (II)	154.415 (II)
IX	3p−4d	...	...	...	154.4410 (II)	154.454 (II)
IX	3p−4d	...	...	...	155.2620 (II)	155.290 (II)
IX	3p−4d	...	...	...	155.5240 (II)	...
VIII	3s−4p	2.3	317.8	100	158.9210 (II)	158.9211 (II)
XIII	2s−2p	2.4	318.2	100	159.0890 (II)	159.077 (II)
VIII	3s−4p	...	...	...	159.1750 (II)	159.1746 (II)
Unidentified lines						
...	...	1.15	280.1	150	...	...
...	...	10	281.9	100	...	...
...	...	1.3	283.5	150	...	...
...	...	3.6	284.2	100	...	...
...	...	0.39	285.6	200	...	...
...	...	0.39	286.3	200	...	...
...	...	0.45	290.4	200	...	...
...	...	0.55	292.5	200	...	...
...	...	0.56	295.1	200	...	...
...	...	1.9	297.6	100	...	...
...	...	2.6	298.8	100	...	...
...	...	3.4	300.1	100	...	...
...	...	0.55	300.9	200	...	...
...	...	0.46	301.4	200	...	...
...	...	1.1	303.0	150	...	...
...	...	0.38	304.9	200	...	...
...	...	0.4	310.0	100	...	...
...	...	0.2	310.9	200	...	...
...	...	0.1	314.5	200	...	...

Notes. The unknown Ar lines may technically originate in spectra up to Ar IX.

References. [(a)] From the CHIANTI database v.8 (Del Zanna et al. 2015); [(b)] from the on-line database at NIST (Kramida et al. 2012).

Table A.6. Iron lines observed in EBIT within the wavelength band λ280 to λ320.

Spectrum	Transition type	Line intensity	λ (Å) This work	Unc. (mÅ)	λ (Å) CHIANTI[a]	λ (Å) NIST[b]
Known lines						
XV	3s−3p	10	284.1	100	284.1630	284.164
XIII	3s−3p	0.21	318.0	100	318.1300	318.21

Notes. The other about 90 lines named in the literature were too weak individually to be distinguished in our spectra.

References. [(a)] From the CHIANTI database v.8 (Del Zanna et al. 2015); [(b)] from the on-line database at NIST (Kramida et al. 2012).

Table A.7. Nickel lines observed in EBIT within the wavelength band λ280 to λ320.

Spectrum	Transition type	Line intensity	λ (Å) This work	Unc. (mÅ)	λ (Å) CHIANTI[a]	λ (Å) NIST[b]
Known lines						
XVII	3s−3p	...	...	...	285.6161	...
XIV	3s−3p	0.12	285.7	150	...	285.878
XVI	3s−3p	2	288.2	100	288.1650	288.149
XIV	3s−3p	1.1	288.5	100	288.7072	...
XIV	3s−3p	...	...	...	...	288.894
XVII	3s−3p	0.68	289.7	100	289.7431	289.743
XIII	3s−3p	...	...	...	290.5660	290.574
XVIII	3s−3p	10	291.9	100	291.9840	291.985
XIV	3s−3p	...	...	...	292.3001	...
XIV	3s−3p	2	292.3	100	...	292.399
XII	3s−3p	0.45	295.3	100	295.3210	295.321
XIV	3s−3p	...	...	...	...	295.555
XIV	3s−3p	5.2	296.8	100	296.9505	...
XV	3s−3p	0.2	298.1	100	298.1510	298.15
XIV	3s−3p	0.55	302.3	100	302.2719	302.264
XIII	3s−3p	0.55	302.7	100	302.8340	302.844
XVI	3s−3p	1.5	304.5	100	304.5070	...
XIII	3s−3p	...	...	...	308.0590	308.049
XIII	3s−3p	2.2	308.4	100	308.5510	308.542
XVI	3s−3p	1.5	309.1	100	309.1790	309.196
XVI	3s−3p	...	...	...	309.6900	...
XV	3s−3p	...	...	...	309.9740	...
XV	3s−3p	...	...	...	311.7550	311.756
XV	3s−3p	...	...	...	312.0300	312.030
XVI	3s−3p	...	...	...	313.2220	313.231
XVI	3s−3p	...	...	...	313.7460	313.724
XX	3s−3p	...	...	...	314.1262	...
XIV	3s−3p	...	...	...	316.2548	316.113
XVI	3s−3p	...	...	...	316.7910	316.811
XII	3s−3p	...	...	...	317.4750	317.475
XV	3s−3p	0.5	319.1	100	319.0630	319.063
Unidentified lines						
...	...	0.25	282.0	100	...	...
...	...	0.14	282.7	150	...	...
...	...	0.18	283.6	100	...	...
...	...	0.24	284.0	100	...	...
...	...	0.15	287.8	150	...	...
...	...	0.55	289.1	100	...	...
...	...	1.8	290.0	100	...	...
...	...	0.51	291.3	100	...	...
...	...	0.27	293.7	100	...	...
...	...	0.29	294.0	100	...	...
...	...	0.28	294.5	100	...	...
...	...	0.7	297.3	100	...	...
...	...	0.22	300.6	100	...	...
...	...	0.4	301.8	100	...	...
...	...	4	304.2	100	...	...
...	...	0.53	305.5	100	...	...
...	...	1.6	305.8	100	...	...
...	...	0.35	306.2	100	...	...
...	...	0.08	310.1	150	...	...
...	...	0.11	310.3	150	...	...
...	...	0.7	311.9	100	...	...
...	...	0.16	312.4	100	...	...
...	...	1	315.1	100	...	...
...	...	2	315.5	100	...	...
...	...	0.75	315.9	100	...	...
...	...	1.2	316.7	100	...	...
...	...	0.45	317.1	100	...	...
...	...	0.95	319.9	100	...	...

Notes. The unknown Ni lines can technically originate in spectra up to Ni XI.

References. [(a)] From the CHIANTI database v.8 (Del Zanna et al. 2015); [(b)] from the on-line database at NIST (Kramida et al. 2012).